

Inversion of Supramolecular Chirality by In Situ Hydrolyzation of Achiral Diethylene Glycol Motifs

Shuting Wang, Laiben Gao, Nan Su, Li Yang, Fengli Gao, Xiaoqiu Dou,* and Chuanliang Feng*



Cite This: *J. Phys. Chem. B* 2022, 126, 1325–1333



Read Online

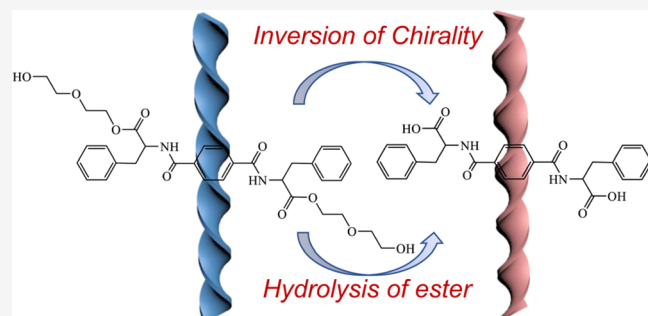
ACCESS |

Metrics & More

Article Recommendations

Supporting Information

ABSTRACT: Chiral inversion of supramolecular assemblies is of great research interest due to its broad practical applications. However, chiral structure transition induced by in situ regulation of building molecules has remained a challenge. Herein, left-handed fibrous assemblies were constructed by C_2 -symmetric L-phenylalanine coupled with diethylene glycol (LPFEG) molecules. In situ hydrolyzing terminal diethylene glycol motifs in LPFEG successfully inverted the chirality of the nanofibers from left- to right-handedness. The transition of right-handed fibers into left-handed fibers could also be achieved via hydrolyzing DPFEG molecules. Circular dichroism (CD) spectroscopy, 1D and 2D nuclear magnetic resonance (NMR) spectroscopy, and Fourier transform infrared (FT-IR) spectroscopy revealed that the back-folded achiral diethylene glycol played a vital role in L/DPFEG molecular arrangements and removing terminal diethylene glycol could induce the opposite rotation of molecular assemblies. Thanks to this merit, the enantioselective separation of racemic phenylalanine was obtained and the enantiomeric excess (*ee*) values could achieve around $\pm 20\%$ after separation. This study not only provides a new strategy to regulate the chiral structure via dynamic modulation of terminal substituents but also presents a promising application in the field of enantioselective separation.



INTRODUCTION

Supramolecular chirality arises from asymmetric spatial stacking of chiral or achiral molecules, which can be found in many supramolecular systems.^{1–3} Dynamic inversion of supramolecular chirality usually offers an effective strategy to regulate chiral structure-related functions (e.g., enantioselective separation,^{4,5} chiral recognition or sensing,^{6,7} asymmetric catalysis,^{8,9} chiral optoelectronics,^{10,11} and biomedicine^{12–14}). Despite the fact that the dynamic inversion of supramolecular chirality has been achieved via co-assembling with other molecules,^{15–18} coordinating with metal ions,^{19–21} varying assembling temperature,^{22,23} light irradiation,^{24,25} and regulation of solvent polarity,^{26–28} it has remained a challenge to realize helicity inversion via in situ modulation of building molecules due to the subtle balance between intermolecular attraction and repulsion easily disturbed by altering the molecular structure of building units. However, regulation of molecular structure often accompanies with new chemical function, and thus dominating the handedness of supramolecular helix by in situ adjustment of molecular substituents is very important and urgently demanded, which will present a novel strategy to develop functional chiral materials.

The side-chain substituent of building unit is closely related to the assembly morphology due to the effect of side-chain interaction on molecular stacking.^{29,30} For example, the amino acid substitution has been found to be involved with the handedness of helical aggregates.^{31–33} The chirality of amino

acids determines twist orientation of chiral structures via transformation of molecular chirality into a microscopic spiral.³⁴ Besides chiral substituents, introduction of achiral motifs (e.g., oligo(ethylene glycol)) can also trigger chirality inversion of helical nanostructures via altering stacking mode of the assembled building molecules.³⁵ However, these examples mainly focus on synthesizing monomer molecules containing distinctive substituents to obtain different chiral structures. Dynamic regulation of side chains in building blocks to in situ modulate the handedness of chiral structures has been rarely reported so far. It is highly desirable in artificial supramolecular system, which is important and necessary to understand the fundamental function and develop practical application of structural transformation and chiral inversion.

Herein, a dynamic chiral inversion of supramolecular nanofibers is achieved by hydrolyzation of phenylalanine-substituted achiral diethylene glycol motifs. C_2 -symmetric L-phenylalanine coupled with diethylene glycol (LPFEG) molecules self-assemble into left-handed (*M*-type) helical

Received: November 23, 2021

Revised: January 20, 2022

Published: February 3, 2022



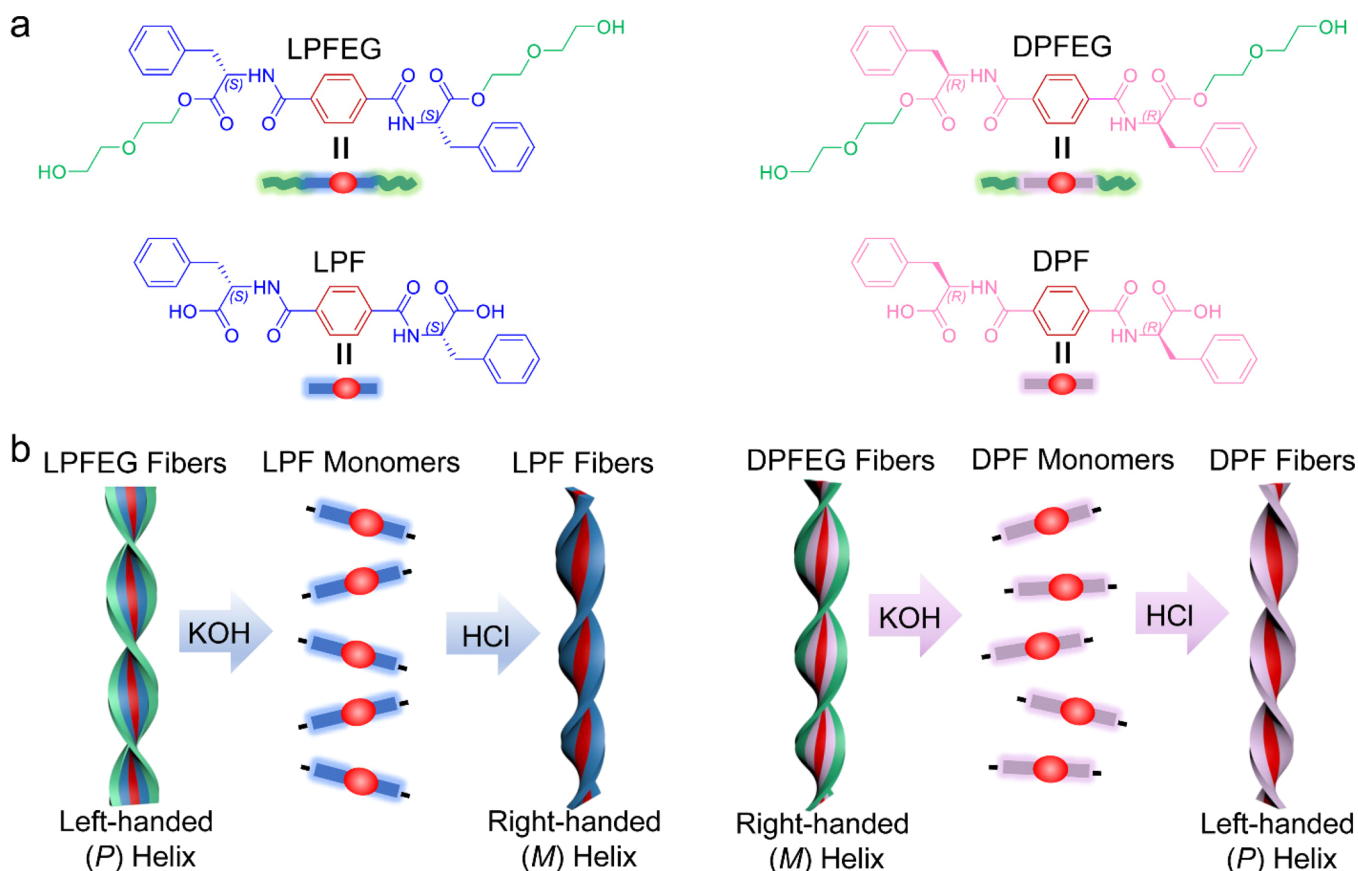


Figure 1. (a) Molecular structures of L/DPFEG and L/DPF. (b) Subsequent addition of KOH and HCl solutions makes the hydrolyzation of terminal diethylene glycol.

fibers, whereas DPFG molecules originated from D-phenylalanine derivatives aggregate into nanofibers with right-handedness (*P*-type) (Figure 1a). After hydrolyzation of terminal diethylene glycol, a helix-to-helix structural transition from *P* into *M* (or from *P* into *M*) is triggered (Figure 1b). Circular dichroism (CD) spectroscopy, 1D and 2D nuclear magnetic resonance (NMR) spectroscopy, and Fourier transform infrared (FT-IR) spectroscopy reveal that the back-folded achiral diethylene glycol plays a vital role in L/DPFEG molecular arrangements, and removing terminal diethylene glycol induces the opposite rotation of molecular assemblies. This chiral fibrous network with dynamic helicity transition provides an attractive candidate for the application of chiral separation. It is found that left-handed LPFEG fibrous film prefers adsorbing D-phenylalanine molecules from the racemic phenylalanine mixtures, and the D-phenylalanine release is activated by transformation of helical fiber structure. The enantiomeric excess (*ee*) values of phenylalanine separation solutions could achieve around $\pm 20\%$. Regulating spiral direction of nanofibers by in situ altering molecular structure of building block realizes that the adsorbed chiral molecules could be released, leading to the obtainment of chiral separation solution with both positive and negative *ee* values by only using single-chirality fibers. For most reported chiral separation materials, solutions with both positive and negative *ee* values are difficult to be obtained by utilizing single chirality materials. This study not only offers a novel approach to realize chiral structural transition via dynamic regulation of terminal substituents but also presents a cost-effective method in the field of chiral separation.

MATERIALS AND METHODS

Materials. 1,4-Benzenedicarbonyl dichloride, L/D-phenylalanine methyl ester hydrochloride, L/D-phenylalanine, and diethylene glycol were purchased from Aladdin Chemical Co., Ltd. Triethylamine (Et_3N), dichloromethane (DCM), dimethyl sulfoxide (DMSO), sodium hydroxide (NaOH), hydrochloric acid (HCl), and other chemical reagents and solvents were purchased from Sinopharm Chemical Reagent Co., Ltd. All chemicals were used without further purification.

Synthesis of L/DPF and L/DPFEG. In ice-bath, 1,4-benzenedicarbonyl dichloride (6.00 g, 27.82 mmol) dissolved in dichloromethane (DCM, 50 mL) was added dropwise to a solution of L-phenylalanine methyl ester hydrochloride (2.6 g, 12.81 mmol) and triethylamine (Et_3N , 10.00 mL, 72.88 mmol) in dry DCM (200 mL). The mixture was stirred at room temperature for 24 h. The solute substances obtained after rotatory evaporation were collected and dried to give dimethyl ester of LPF. Aqueous sodium hydroxide (2 M, 10 mL) was added to the dimethyl ester of LPF in methanol (20 mL). The mixture was stirred for 24 h at room temperature until a clear solution was obtained. The solution was then acidified with 3.0 M hydrochloric acid until pH value reached no more than 3.0 and white gel-like sediment was formed. The gel phase was filtered, washed with deionized water, and finally dried in the infrared drying oven to give LPF (3.70 g, 62.8%). ^1H NMR (500 MHz, $\text{DMSO}-d_6$) δ 3.07–3.20 (4H, CH_2), 4.62 (2H, CH), 7.16–7.35 (10H, $=\text{CH}$), 7.84 (4H, $=\text{CH}$), 8.83 (2H, NH), 12.81 (2H, COOH). EI-MS for $\text{C}_{26}\text{H}_{24}\text{O}_{6}\text{N}_2$ calcd 460.16; found 459.16 [$\text{M}-\text{H}^-$]. Elemental analysis for

$C_{26}H_{24}O_6N_2$ calcd C: 67.82%, H: 5.25%, N: 6.08%, O: 20.85%; found C: 67.69%, H: 5.44%, N: 5.94%, O: 21.03%.

Concentrated hydrochloric acid (1 mL) was added dropwise to a mixture of LPF (1.70 g, 3.69 mmol) and diethylene glycol (40 mL). The mixture was stirred at 145 °C for 4 h. After the reaction, the solution was added into the ice-water mixture, and a white gel-like sediment was formed. LPFEG (1.50 g, 77.4%) was obtained after filtering, repeatedly washing the sediment with deionized water, and drying in the infrared drying oven. 1H NMR (500 MHz, DMSO- d_6) δ 3.04–3.24 (4H, CH₂), 3.41–3.50 (8H, CH₂), 3.54–3.63 (4H, CH₂), 4.20 (4H, CH₂), 4.60 (2H, CH), 4.69 (2H, OH), 7.18–7.34 (10H, =CH), 7.86 (4H, =CH), 8.96 (2H, NH). EI-MS for $C_{34}H_{40}O_{10}N_2$ calcd 636.27; found 635.26 [M–H][−]. Elemental analysis for $C_{34}H_{40}O_{10}N_2$ calcd C: 64.14%, H: 6.33%, N: 4.40%, O: 25.13%; found C: 63.86%, H: 6.58%, N: 4.24%, O: 25.35%.

DPF and DPFEG molecules merely replaced L-phenylalanine methyl ester hydrochloride with D-phenylalanine methyl ester hydrochloride. DPF 1H NMR (500 MHz, DMSO- d_6) δ 3.07 (2H, CH), 3.21 (2H, CH), 4.63 (2H, CH), 7.15–7.35 (10H, =CH), 7.84 (4H, =CH), 8.83 (2H, NH), 12.81 (2H, COOH). EI-MS for $C_{26}H_{24}O_6N_2$ calcd 460.16; found 459.16 [M – H][−]. Elemental analysis for $C_{26}H_{24}O_6N_2$ calcd C: 67.82%, H: 5.25%, N: 6.08%, O: 20.85%; found C: 67.63%, H: 5.41%, N: 5.85%, O: 21.07%.

DPFEG 1H NMR (500 MHz, DMSO- d_6) δ 3.06–3.22 (4H, CH₂), 3.42–3.48 (8H, CH₂), 3.55–3.63 (4H, CH₂), 4.19 (4H, CH₂), 4.58 (2H, CH), 4.68 (2H, OH), 7.17–7.35 (10H, =CH), 7.85 (4H, =CH), 8.98 (2H, NH). EI-MS for $C_{34}H_{40}O_{10}N_2$ calcd 636.27; found 635.26 [M–H][−]. Elemental analysis for $C_{34}H_{40}O_{10}N_2$ calcd C: 64.14%, H: 6.33%, N: 4.40%, O: 25.13%; found C: 63.89%, H: 6.47%, N: 4.22%, O: 25.45%.

NMR Spectroscopy and Electron Ionization Mass (EI-MS) Spectrometry. 1H nuclear magnetic resonance (1H NMR) spectroscopy was performed on a Bruker Advance III 400 Instrument. 2D NMR spectra were recorded on Bruker Advance III 400 Instrument. NMR spectra were taken in DMSO- d_6 or D₂O. EI-MS spectra were recorded on a Waters Q-ToF Mass Instrument. Methanol was used as the solvent. The 1H NMR and EI-MS spectra of L/DPF and L/DPFEG are presented in Figures S1–S8.

Elemental Analysis. Elemental analysis for C, N, and H was performed on a vario EL cube elementar (Germany). Elemental analysis for O was performed on a Thermo Scientific FlashSmart Elemental Analyzer (USA).

Hydrogel Preparation. By heating suspensions of LPF (2 mg/mL) to 90–95 °C until forming clear solution and then cooling them down to 20 °C, LPF molecules can self-assemble into hydrogel. DPF, LPFEG, and DPFG hydrogels were prepared in the same way.

CD Spectroscopy. CD spectra were recorded on a JASCO J-1500 CD spectrometer using a 1 mm quartz cuvette. All scans of samples were performed in the UV region (190–500 nm) with a data pitch of 0.5 nm at room temperature. Temperature-dependent CD spectra were performed at 1 °C/min from 25 to 90 °C.

Ultraviolet–Visible (UV–Vis) Spectroscopy. UV–vis spectra were measured using a Thermo SCIENTIFIC EVOLUTION 201 instrument. Diluted gels (0.1 wt %) and EtOH solutions of gelators. Data between wavelengths of 190

and 500 nm were collected with a data pitch of 1 nm at room temperature.

X-Ray Diffraction (XRD) Study. The XRD patterns of L/DPFEG and L/DPF assemblies were obtained from dried L/DPFEG and L/DPF gel powders. The preparation of hydrogels was mentioned above. The dried gel powders were obtained by drying hydrogels under 40 °C. The XRD patterns were recorded on a Bruker D8 ADVANCE with DAVINCI instrument.

Scanning Electron Microscopy (SEM). The morphologies of the LPF, DPF, LPFEG, DPFEG hydrogels and solutions were imaged using an FEI QUANTA 250 SEM (USA). Samples were prepared by depositing dilute solutions (approximately 0.5 mg/mL) of gel on the silicon slice. After drying under vacuum, the samples were coated with 8–10 nm of Au on a sputtering coater (S 150B, Edwards, UK). The diluted hydrogel (0.5 mg/mL) was prepared by adding 3 mL of deionized water on the top of 1 mL of hydrogel (2 mg/mL) and mixing them homogeneously.

Fourier Transform Infrared (FT-IR) Spectroscopy. FT-IR spectra of LPFEG and LPF assemblies were recorded on a Bruck EQUINOX55 instrument. The KBr pelleting technique was used for preparation of powder samples. The FT-IR spectra were performed between 4000 and 400 cm^{−1} at an interval of 1.9285 cm^{−1}.

Ultrahigh-Performance Liquid Chromatography (UPLC) Spectrometry. To study the hydrolyzation of LPFEG molecules, the samples were analyzed using an UPLC-MS instrument (UPLC 30A/Sciex Quadrupole 5500, USA). Methanol was used as the solvent for UPLC test.

Analysis of ee. To quantitatively analyze the ee value of phenylalanine solution, ee calibration curve was created. The total concentration of phenylalanine solution was fixed at 0.4 mM. The ee values for the experimental solutions were 100, 80, 60, 40, 20, 0, −20, −40, −60, −80, and −100%. The ee value is calculated by $([L\text{-Phe}] - [D\text{-Phe}]) / ([L\text{-Phe}] + [D\text{-Phe}]) \times 100\%$. Herein, the equal volume of deionized water instead of racemic Phe solution was added on the LPFEG fibrous film as the control group. To avoid the effect of leaking gelators on the CD intensity, the CD intensity at 215 nm was obtained by subtracting control group from the experimental group.

Chiral Separation of Racemic Phenylalanine. Two hundred microliters of the LPFEG hot solution (around 90 °C) was added in a 14-mm-diameter petri dish. The solution transformed into transparent hydrogel after cooling down to 20 °C for 30 min. After drying under 45 °C, the LPFEG nanofibers were deposited on the petri dish surface. Then, 1 mL of racemic phenylalanine solution (the molar ratio of L-phenylalanine and D-phenylalanine was 1:1, the total concentration of phenylalanine solution was 0.4 mM). After 48 h, the supernatant was collected. Then, 1 mL of KOH solution was added in the petri dish. After 24 h, the LPFEG fibrous films disappeared. The addition of 20 μL of concentrated HCl resulted in the formation of LPF fibrous floccules. The filtrate was immediately collected. The ee values of the supernatant and the filtrate were determined according to the CD signal at 215 nm.

RESULTS AND DISCUSSION

The C_2 -symmetric phenylalanine-derived molecules L/DPF and L/DPFEG were synthesized through a conventional liquid phase reaction in two or three steps according to Scheme S1. These four molecules self-assembled into hydrogels in

deionized water (2 mg/mL) via heating the samples to 90–95 °C and cooling them down to 20 °C (Figure S9). The inner structures of hydrogels were investigated by SEM. The diluted hydrogels (0.5 mg/mL) were deposited on silicon wafers and dried at 20 °C under vacuum. It was observed that both LPFEG (Figure 2a) and DPF (Figure 2b) molecules

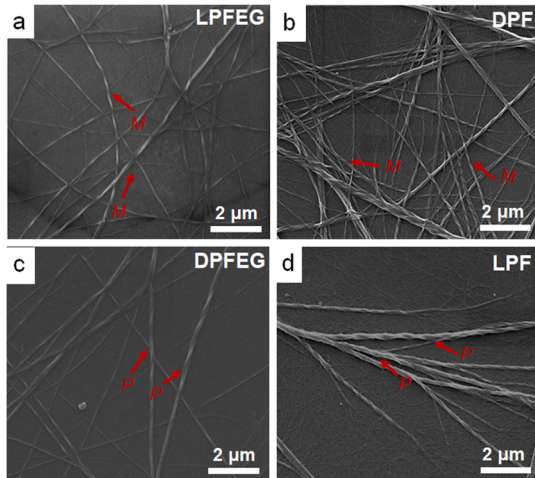


Figure 2. SEM images of (a) left-handed (*M*) helical LPFEG, (b) left-handed (*M*) twisted DPF, (c) right-handed (*P*) helical DPFEGL, and (d) right-handed (*P*) twisted LPF nanofibers in the self-assembled hydrogels.

aggregated into left-handed (*M*-type) nanofibers, whereas both DPFEGL (Figure 2c) and LPF (Figure 2d) molecules formed right-handed (*P*-type) nanofibers. The diameter and helical pitch of L/DPFEGL nanofibers were around 120–150 nm and 600–900 nm, respectively. The twisted nanofibers with 90–200 nm in width and 150–260 nm in helical pitch were observed for L/DPF. Although LPFEG and LPF derived from L-phenylalanine, their twisted assemblies displayed a completely opposite rotatory direction. The opposite handedness of helical nanofibers was also found between DPFEGL and DPF, although both molecules possessed the same D-phenylalanine residue. By contrast, all these four molecules were well dissolved in methanol (MeOH) (Figure S10). Due to molecular interactions disturbed by MeOH solvent,^{36,37} unordered L/DPFEGL and L/DPF aggregates were formed (Figure S11) after evaporation of MeOH.

The helicity structure formed by L/DPFEGL and L/DPF molecular building units in the gel state was further investigated by UV-vis and CD spectroscopy. Herein, the concentrations of L/DPFEGL samples were kept at 3.1 mmol/L, and the concentrations of L/DPF were kept at 4.3 mmol/L. The maximum UV absorbance at 245–247 nm for L/DPFEGL and L/DPF molecules blue-shifted to 238–240 nm for L/DPFEGL and L/DPF assemblies corroborated the *J*-type $\pi-\pi$ aggregation of molecules in the supramolecular assemblies (Figure S12).^{38,39} For CD results, LPFEG assemblies in hydrogels displayed a considerable negative CD signal at 229 nm and a strong CD peak at 273 nm. Compared with LPFEG assemblies, the LPFEG molecules dissolved in MeOH (Figure 3a) displayed a significantly reduced positive Cotton effect at 218 nm and a negative Cotton effect at 238 nm (Figure 3b). Although the effective concentrations of LPFEG in H₂O and MeOH were kept constant (3.1 mmol/L), the CD intensity of LPFEG assemblies was almost five times higher than the

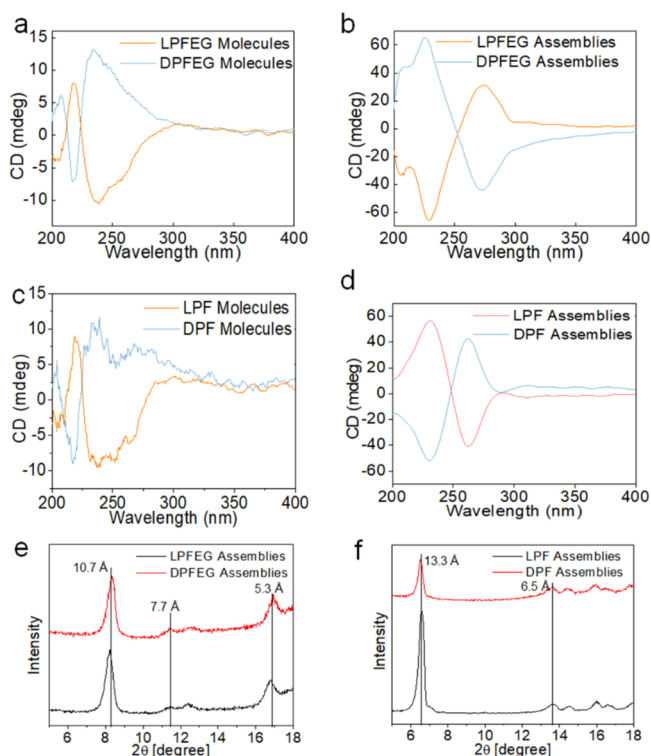


Figure 3. CD spectra of (a) L/DPFEGL assemblies in H₂O, (b) L/DPFEGL molecules in MeOH, (c) L/DPF assemblies in H₂O, and (d) L/DPF molecules in MeOH obtained by using a 1 mm path length of a quartz cuvette. The concentrations of L/DPFEGL samples were 3.1 mmol/L, and the concentrations of L/DPF samples were 4.3 mmol/L. XRD patterns of (e) L/DPFEGL assemblies and (f) L/DPF assemblies obtained from H₂O.

molecular CD signal intensity in the region of 210–300 nm. The shifted and enhanced CD peaks from LPFEG molecules to assemblies indicated that LPFEG assemblies possessed not only molecular chirality but also supramolecular structural chirality.⁴⁰ For LPF assemblies in hydrogels, a positive Cotton effect at 230 nm and a negative Cotton effect at 262 nm were detected (Figure 3c). The apparent inverted CD patterns between LPFEG and LPF assemblies corresponded to their opposite handedness in the assembled nanofibers as observed in the SEM images. Interestingly, the CD spectrum of LPF molecules was very similar to the CD spectrum of LPFEG, in which a positive peak exhibited at 218 nm and a negative peak appeared at 243 nm (Figure 3d). It suggested that LPFEG and LPF molecules presented almost an identical chiroptical activity when the same L-phenylalanine moieties symmetrically centered with benzene core. The supramolecular chirality inversion was also found between DPFEGL and DPF assemblies. The molecular chirality in CD spectra of DPFEGL and DPF almost kept the same, even if terminal groups of DPFEGL and DPF were diethylene glycol and carboxylic acid, respectively. XRD measurements were used to reveal the molecular arrangements of L/DPFEGL and L/DPF assemblies. The XRD patterns of L/DPFEGL assemblies showed three characteristic peaks at 10.7, 7.7, and 5.3 Å (corresponding to the ratio of 1:1/ $\sqrt{2}$:1/2), indicating the square packing mode (Figure 3e).⁴¹ For L/DPF assemblies, the XRD peaks at 13.3 and 6.5 Å (corresponding to the ratio of 1:1/2) suggested a lamellar aggregation with a *d*-spacing of 13.3 Å (Figure 3f).⁴² According to the CD, UV-vis, and XRD results, it was

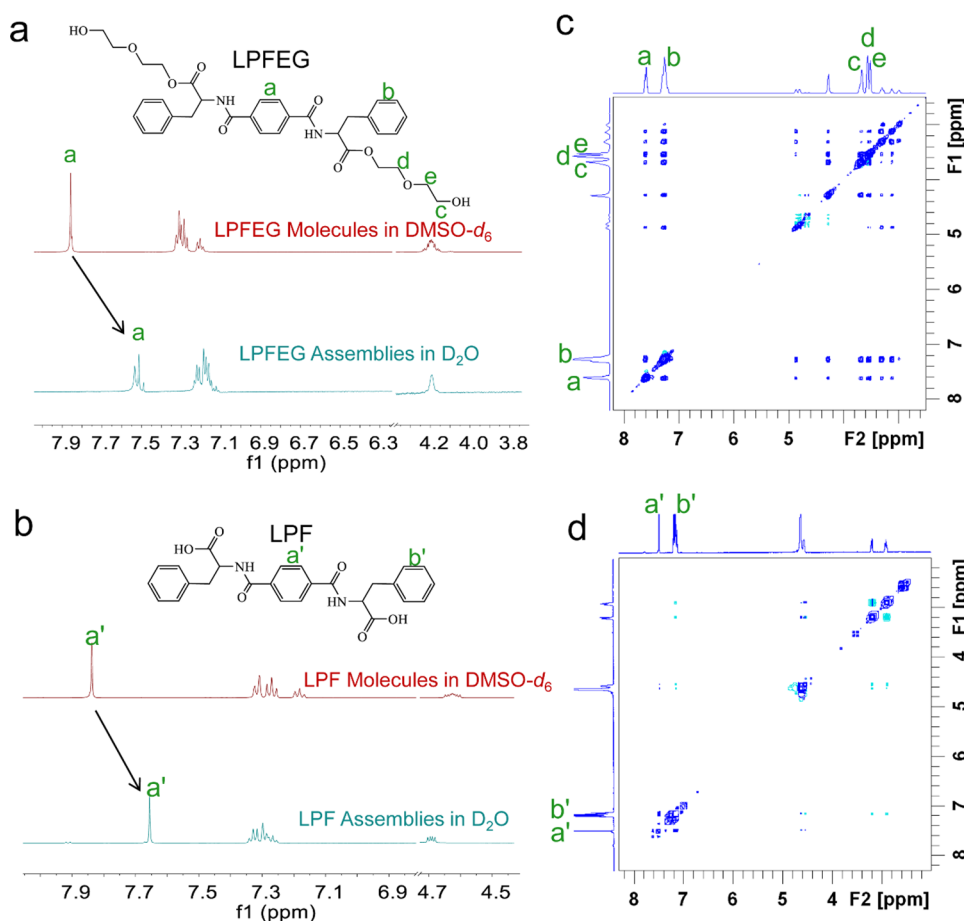


Figure 4. (a) ^1H NMR spectra of LPFEG molecules in $\text{DMSO}-d_6$ and LPFEG assemblies in D_2O . (b) ^1H NMR spectra of LPF molecules in $\text{DMSO}-d_6$ and LPF assemblies in D_2O . (c) NOESY spectrum of LPFEG assemblies in D_2O . (d) NOESY spectrum of LPF assemblies in D_2O .

apparent that terminal diethylene glycol groups regulated the molecular arrangements. To investigate the thermal stability of L/DPFEG and L/DPF assemblies, temperature-dependent CD measurements were applied. When the temperature was above 50 °C, the CD signals of L/DPFEG and L/DPF gradually decreased, indicating the disassembly of L/DPFEG and L/DPF (Figure S13). The CD spectra of L/DPFEG and L/DPF only showed signals of molecular chirality when the temperature reached around 90 °C, suggesting the transformation from L/DPFEG and L/DPF assemblies to L/DPFEG and L/DPF molecules.

To reveal the intermolecular interactions in the supramolecular assemblies, 1D and 2D ^1H NMR spectroscopy and Fourier transform infrared (FT-IR) spectroscopy were carried out. Herein, LPFEG and LPF were chosen as representative molecules to do characterization. The monomeric state of LPFEG and LPF was achieved by dissolving molecules in dimethyl sulfoxide ($\text{DMSO}-d_6$). Compared with the monomeric LPFEG and LPF in $\text{DMSO}-d_6$, the protons (H_a in LPFEG, $\text{H}_{a'}$ in LPF) at the periphery of the central benzene core showed obvious upfield shifts in the self-assemblies dispersed in D_2O (LPFEG: around 7.86 ppm in $\text{DMSO}-d_6$ and 7.51 ppm in D_2O ; LPF: around 7.84 ppm in $\text{DMSO}-d_6$ and 7.65 ppm in D_2O) (Figure 4a,b). These chemical shifts were attributed to the increased electron density caused by $\pi-\pi$ stacking between central benzene rings.⁴³ In FT-IR spectra (Figure S14), the amide I band at 1641 cm^{-1} for LPFEG assemblies and at 1622 cm^{-1} for LPF assemblies, the amide II

band at 1544 cm^{-1} for LPFEG assemblies and at 1549 cm^{-1} for LPF assemblies implied the $\text{N}-\text{H}\cdots\text{O}=\text{C}$ hydrogen-bonding associations in both LPFEG and LPF assemblies. The N–H stretching vibration at 3239 cm^{-1} for LPFEG assemblies and 3315 cm^{-1} for LPF assemblies confirmed the hydrogen bonds between the amide groups.^{44,45} Herein, $\pi-\pi$ stacking between benzene cores and hydrogen bonding between amide groups cooperatively drove the supramolecular assemblies. The spatial structures of aggregated molecules were subsequently detected via 2D nuclear Overhauser enhancement spectroscopy (NOESY). Nuclear Overhauser effect (NOE) peaks between the protons of the central benzene moiety ($\text{H}_a/\text{H}_{a'}$) and the protons of peripheral benzene unit ($\text{H}_b/\text{H}_{b'}$) were observed in both LPFEG and LPF assemblies (Figure 4c,d), which may be caused by a slightly rotated offset between monomers in these two stacked systems.⁴⁶ In addition, the intermolecular cross-peaks between the benzene core protons (H_a) and the glycol protons ($\text{H}_d/\text{H}_e/\text{H}_c$) in LPFEG assemblies indicated the presence of back-folded conformation of diethylene glycol side chains. According to the NMR results, it was reasonably speculated that the back-folded diethylene glycol induced an opposite rotation in molecular arrangement, further leading to the handedness inversion of helical assemblies.

The opposite helical twist direction in LPFEG and LPF nanofibers inspired us to realize the helix inversion via removing diethylene glycol side chains in LPFEG. To break linkage between diethylene glycol and phenylalanine, basic

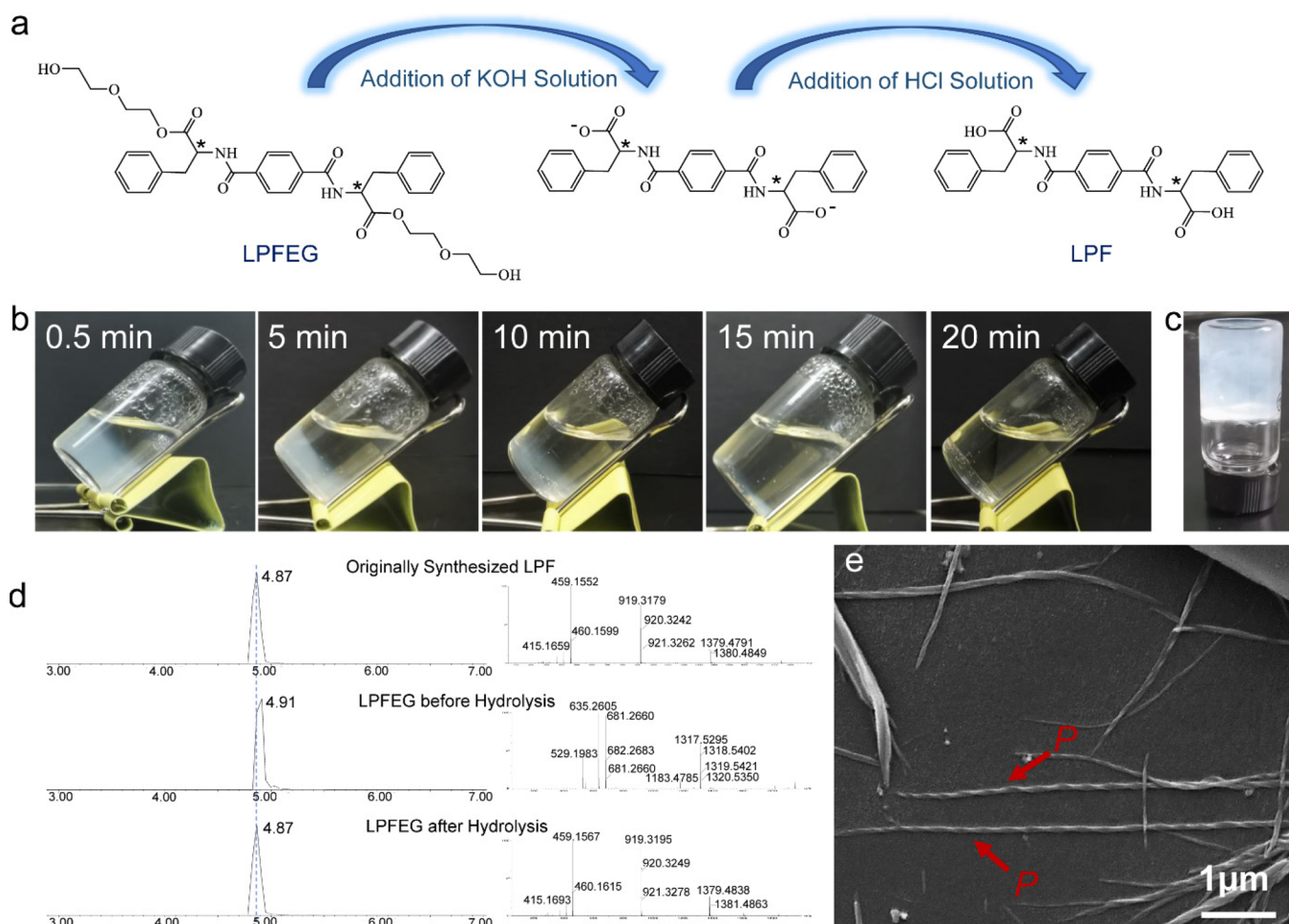


Figure 5. (a) Chemical transformation of LPFEG molecule into LPF molecule upon addition of KOH and HCl solution. (b) Disassembled LPFEG hydrogel in alkaline environment. (c) LPF hydrogel formed after hydrolyzing LPFEG molecules. (d) UPLC chromatograms and mass spectra for selected spiked compounds. Upper: originally synthesized LPF molecules; middle: LPFEG before hydrolysis; lower: LPFEG after hydrolysis. (e) SEM image of right-handed nanofibers in the LPF hydrogel formed after hydrolyzing LPFEG molecules.

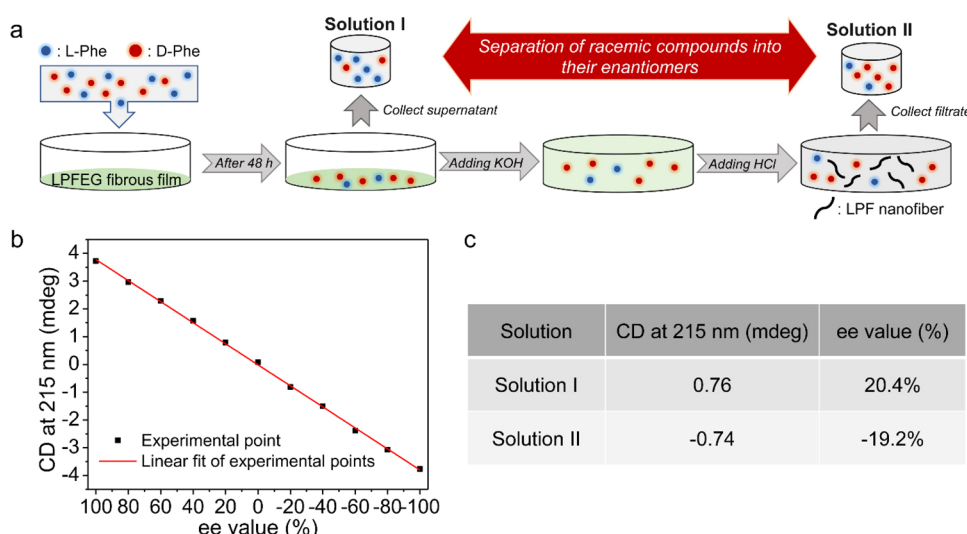


Figure 6. (a) A schematic diagram of separating racemic phenylalanine molecules into their enantiomers by utilizing the inversion of chiral structure in LPFEG nanofibers. (b) Black points represent CD signal at 215 nm with varying ee values for phenylamine solution (0.4 mM). Red line means linear fit of black experimental points ($y = 0.03788x - 0.01438$, $R^2 = 0.99938$). (c) ee calculations of solution I and solution II.

hydrolysis of esters in LPFEG molecules was applied (Figure 5a). With the addition of KOH aqueous solution (1 mL, 100

mg/mL) on the top of LPFEG hydrogel (2 mL, 2 mg/mL), the white LPFEG hydrogel gradually disappeared (Figure 5b).

A clear solution was obtained around 20 min, indicating that diethylene glycol was successfully removed from LPFEG molecules. In the alkaline solution, the deprotonation of terminal carboxylate moieties introduced negative interfacial charges, and thereby strong repulsive electrostatic interactions between molecules resulted in the disassembly of hydrogel aggregates. The formation of hydrogel was achieved via adding the HCl solution (3 mol/L) to protonate carboxylic acids (final pH value around 2, Figure 5c). The UPLC analyses of hydrogel formed after hydrolysis corroborated that LPFEG hydrogel transformed to LPF hydrogel (Figure 5d). The SEM and CD measurements demonstrated that dynamic handedness inversion of hydrogel fibers was realized via regulation of side chains in molecular units (before hydrolysis: left-handed nanofibers; after hydrolysis: right-handed nanofibers, Figures 5e and S15). The effect of K⁺ ions on the chiroptical activities of L/DPF assemblies was also investigated. The L/DPF assemblies formed in KCl solution exhibited the same CD spectra as those formed in deionized water (Figure S16), which indicated that the addition of K⁺ ions did not change the chiroptical activities of L/DPF assemblies.

The inversion of chiral structure triggered by the removal of diethylene glycol from L/DPFEG molecules provides a potential strategy for enantioselective separation. Herein, left-handed helical LPFEG nanofibers were deposited on the petri dish to investigate their enantioselective separation performance (Figure 6a). The 1:1 mixture of L-phenylalanine (L-Phe) and D-phenylalanine (D-Phe) was firstly added onto the LPFEG fibrous film. After 48 h, the enantiomeric excess (ee) value of the supernatant (labeled as solution I) achieved to 20.4%, which no longer increased with the extension of time. The result suggested that left-handed LPFEG nanofibers preferred capturing D-Phe molecules, since the chiral spatial conformation of fibrous assembly would affect the contacting area and binding interactions with phenylamine.^{4,47} To collect phenylalanine molecules absorbed on LPFEG films, KOH solution was applied. With the hydrolysis of LPFEG molecules, the fibrous assemblies disassembled, and the adsorbed phenylalanine molecules were released in the solution. Regulating the solution pH into acid condition generated right-handed LPF fibrous floccules. The phenylalanine molecules adsorbed on LPFEG fibers were collected after immediately filtering the above solution (the filtrate was labeled as solution II). The ee value of solution II was detected to be -19.2% (Figure 6b,c). For most chiral materials used for enantioselective separation,^{48,49} the adsorbed chiral molecules are difficult to be released, which means we should use two kinds of chiral materials constructed by enantiomeric molecules to get the solutions with both positive and negative ee values. Herein, the handedness of fibers can be inverted by in situ hydrolyzation of diethylene glycol motifs. Thanks to this merit, the chiral molecules adsorbed on the chiral fibers can be released with the inversion of spiral direction of chiral fibers. Therefore, the solutions with both positive and negative ee values can be obtained by only using single chiral gelators. Although the ee values of solutions I and II remain to be improved, this result demonstrates that the inversion of chiral structure in supramolecular nanofibers is indeed valuable for chiral separation applications.

CONCLUSIONS

In conclusion, the chiral structure in supramolecular assembly was regulated by modulating the side motifs of building units.

Compared with L/DPF assemblies, the back-folded diethylene glycol in L/DPFEG assemblies plays an important role in the inversion of chiral structure. Hydrolyzation of diethylene glycol substituents in L/DPFEG molecules successfully triggered that L/DPFEG chiral assemblies transformed into L/DPF helical nanofibers with opposite spiral direction. Moreover, these supramolecular assemblies with helical inversion have been utilized for the enantioselective separation of racemic phenylalanine mixture. This study not only realizes the regulation of supramolecular chirality by in situ dominating terminal substituents of building molecules, but also provides a potential strategy for enantioselective separation.

ASSOCIATED CONTENT

Supporting Information

The Supporting Information is available free of charge at <https://pubs.acs.org/doi/10.1021/acs.jpcb.1c10018>.

Synthesis process of L/DPFEG and L/DPF molecules (Scheme S1); ¹H NMR and EI-MS spectra of L/DPFEG and L/DPF molecules (Figures S1–S8); photographic images of L/DPFEG and L/DPF hydrogels (Figure S9); photographic images of L/DPFEG and L/DPF methanol solution (Figure S10); the SEM images of L/DPFEG and L/DPF unordered aggregates (Figure S11); UV spectra of L/DPFEG and L/DPF (Figure S12); Temperature-dependent CD spectra (Figure S13); FT-IR spectra of L/DPFEG and L/DPF (Figure S14); CD spectrum of hydrogel formed after hydrolyzing LPFEG (Figure S15); CD spectra of L/DPF assemblies formed in KCl solution (Figure S16) ([PDF](#))

AUTHOR INFORMATION

Corresponding Authors

Xiaoqiu Dou – State Key Laboratory of Metal Matrix Composites, Shanghai Key Laboratory for Molecular Engineering of Chiral Drugs, School of Materials Science and Engineering, School of Materials Science and Engineering, Shanghai Jiao Tong University, Shanghai 200240, China; Email: douxiaoqiu@sjtu.edu.cn

Chuanliang Feng – State Key Laboratory of Metal Matrix Composites, Shanghai Key Laboratory for Molecular Engineering of Chiral Drugs, School of Materials Science and Engineering, School of Materials Science and Engineering, Shanghai Jiao Tong University, Shanghai 200240, China; orcid.org/0000-0001-6137-5568; Email: clfeng@sjtu.edu.cn

Authors

Shuting Wang – State Key Laboratory of Metal Matrix Composites, Shanghai Key Laboratory for Molecular Engineering of Chiral Drugs, School of Materials Science and Engineering, School of Materials Science and Engineering, Shanghai Jiao Tong University, Shanghai 200240, China

Laiwen Gao – State Key Laboratory of Metal Matrix Composites, Shanghai Key Laboratory for Molecular Engineering of Chiral Drugs, School of Materials Science and Engineering, School of Materials Science and Engineering, Shanghai Jiao Tong University, Shanghai 200240, China

Nan Su – State Key Laboratory of Metal Matrix Composites, Shanghai Key Laboratory for Molecular Engineering of Chiral Drugs, School of Materials Science and Engineering,

School of Materials Science and Engineering, Shanghai Jiao Tong University, Shanghai 200240, China

Li Yang — State Key Laboratory of Metal Matrix Composites, Shanghai Key Laboratory for Molecular Engineering of Chiral Drugs, School of Materials Science and Engineering, School of Materials Science and Engineering, Shanghai Jiao Tong University, Shanghai 200240, China

Fengli Gao — State Key Laboratory of Metal Matrix Composites, Shanghai Key Laboratory for Molecular Engineering of Chiral Drugs, School of Materials Science and Engineering, School of Materials Science and Engineering, Shanghai Jiao Tong University, Shanghai 200240, China

Complete contact information is available at:

<https://pubs.acs.org/10.1021/acs.jpcb.1c10018>

Author Contributions

The manuscript was written through contributions of all authors. All authors have given approval to the final version of the manuscript.

Notes

The authors declare no competing financial interest.

ACKNOWLEDGMENTS

The authors gratefully acknowledge the financial support for this research from the National Nature Science Foundation of China (NSFC 51833006, 52003154), Shanghai Pujiang Program (20PJ1407400), Natural Science Foundation of Shanghai (20ZR1425500), Innovation Program of Shanghai Municipal Education Commission (201701070002E00061), SJTU Trans-med Awards Research (No.WF5401X62X603), Science and Technology Commission of Shanghai Municipality (20S31904600).

REFERENCES

- (1) Xing, P. Y.; Zhao, Y. L. Controlling supramolecular chirality in multicomponent self-assembled systems. *Acc. Chem. Res.* **2018**, *51*, 2324–2334.
- (2) Liu, M. H.; Zhang, L.; Wang, T. Y. Supramolecular chirality in self-assembled systems. *Chem. Rev.* **2015**, *115*, 7304–7397.
- (3) Ariga, K.; Mori, T.; Kitao, T.; Uemura, T. Supramolecular chiral nanoarchitectonics. *Adv. Mater.* **2020**, *32*, No. 1905657.
- (4) Zhang, Y. Q.; Qin, M. G.; Zhao, C. L.; Dou, X. Q.; Xing, C.; Sun, M.; Ma, X. Y.; Feng, C. L. Controlled chiral transcription and efficient separation via graphene oxide encapsulated helical supramolecular assembly. *Carbon* **2020**, *165*, 82–89.
- (5) Zhou, C. Q.; Ren, Y. Y.; Han, J.; Xu, Q. Q.; Guo, R. Chiral polyaniline hollow nanotwists toward efficient enantioselective separation of amino acids. *ACS Nano* **2019**, *13*, 3534–3544.
- (6) Yin, P. C.; Zhang, Z. M.; Lv, H. J.; Li, T.; Haso, F.; Hu, L.; Zhang, B. F.; Bacsa, J.; Wei, Y. G.; Gao, Y. Q.; et al. Chiral recognition and selection during the self-assembly process of protein-mimic macroanions. *Nat. Commun.* **2015**, *6*, 6475.
- (7) Mehwish, N.; Dou, X. Q.; Zhao, C. L.; Feng, C. L.; Fu, Q. Chirality transfer in supramolecular co-assembled fibrous material enabling the visual recognition of sucrose. *Adv. Fiber Mater.* **2020**, *2*, 204–211.
- (8) Tan, C. X.; Chu, D. D.; Tang, X. H.; Liu, Y.; Xuan, W. M.; Cui, Y. Supramolecular coordination cages for asymmetric catalysis. *Chem. – Eur. J.* **2019**, *25*, 662–672.
- (9) Zhao, C.; Sun, Q. F.; Hart-Cooper, W. M.; DiPasquale, A. G.; Toste, F. D.; Bergman, R. G.; Raymond, K. N. Chiral amide directed assembly of a diastereo- and enantiopure supramolecular host and its application to enantioselective catalysis of neutral substrates. *J. Am. Chem. Soc.* **2013**, *135*, 18802–18805.
- (10) Wang, F.; Ji, W.; Yang, P.; Feng, C. L. Inversion of circularly polarized luminescence of nanofibrous hydrogels through co-assembly with achiral coumarin derivatives. *ACS Nano* **2019**, *13*, 7281–7290.
- (11) Niu, D.; Jiang, Y. Q.; Ji, L. K.; Ouyang, G. H.; Liu, M. H. Coordination and π -stacking driven self-assembly pathways to inversion and switching of circularly polarized luminescence. *Angew. Chem., Int. Ed.* **2019**, *131*, 6007–6011.
- (12) Jiang, S. J.; Zeng, Q.; Zhao, K.; Liu, J. Y.; Sun, Q. N.; Huang, K.; He, Y.; Zhang, X. H.; Wang, H.; Shi, X. H.; et al. Chirality bias tissue homeostasis by manipulating immunological response. *Adv. Mater.* **2021**, *34*, No. 2105136.
- (13) Sun, N.; Dou, X. Q.; Tang, Z. M.; Zhang, D. D.; Ni, N.; Wang, J. J.; Gao, H. Q.; Ju, Y. H.; Dai, X. C.; Zhao, C. L.; et al. Bio-inspired chiral self-assemblies promoted differentiation of retinal progenitor cells through activation of metabolic pathway. *Bioact. Mater.* **2021**, *6*, 990–997.
- (14) Dou, X. Q.; Mehwish, N.; Zhao, C. L.; Liu, J. Y.; Xing, C.; Feng, C. L. Supramolecular hydrogels with tunable chirality for promising biomedical applications. *Acc. Chem. Res.* **2020**, *53*, 852–862.
- (15) Wang, F.; Qiu, H. B.; Feng, C. L. Wrapping chiral nanoribbons into coiled and condensed microstructures in supramolecular hydrogels. *Adv. Funct. Mater.* **2020**, *30*, No. 2002936.
- (16) Liu, G. F.; Zhu, L. Y.; Ji, W.; Feng, C. L.; Wei, Z. X. Inversion of the supramolecular chirality of nanofibrous structures through co-assembly with achiral molecules. *Angew. Chem., Int. Ed.* **2016**, *55*, 2411–2415.
- (17) Li, P. Y.; Lü, B. Z.; Han, D. X.; Duan, P. F.; Liu, M. H.; Yin, M. Z. Stoichiometry-controlled inversion of circularly polarized luminescence in co-assembly of chiral gelators with an achiral tetraphenylethylene derivative. *Chem. Commun.* **2019**, *55*, 2194–2197.
- (18) Yang, L.; Wang, F.; Aupheudeus, D. Y.; Feng, C. L. Achiral isomers controlled circularly polarized luminescence in supramolecular hydrogels. *Nanoscale* **2019**, *11*, 14210–14215.
- (19) Wang, F.; Feng, C. L. Metal-ion-mediated supramolecular chirality of L-phenylalanine based hydrogels. *Angew. Chem., Int. Ed.* **2018**, *57*, 5655–5659.
- (20) Liu, G. F.; Sheng, J. H.; Teo, W. L.; Yang, G. B.; Wu, H. W.; Li, Y. X.; Zhao, Y. L. Control on dimensions and supramolecular chirality of self-assemblies through light and metal ions. *J. Am. Chem. Soc.* **2018**, *140*, 16275–16283.
- (21) Zhou, X. Q.; Jin, Q. X.; Zhang, L.; Shen, Z. C.; Jiang, L.; Liu, M. H. Self-assembly of hierarchical chiral nanostructures based on metal-benzimidazole interactions: chiral nanofibers, nanotubes, and microtubular flowers. *Small* **2016**, *12*, 4743–4752.
- (22) Huang, Z. G.; Kang, S. K.; Banno, M.; Yamaguchi, T.; Lee, D.; Seok, C.; Yashima, E.; Lee, M. Pulsating tubules form noncovalent macrocycles. *Science* **2012**, *337*, 1521–1526.
- (23) Korevaar, P. A.; de Greef, T. F. A.; Meijer, E. W. Pathway complexity in π -conjugated materials. *Chem. Mater.* **2014**, *26*, 576–586.
- (24) Zhao, D. P.; van Leeuwen, T.; Cheng, J. L.; Feringa, B. L. Dynamic control of chirality and self-assembly of double-stranded helicates with light. *Nat. Chem.* **2017**, *9*, 250–256.
- (25) San Jose, B. A.; Ashibe, T.; Tada, N.; Yorozuya, Z.; Akagi, K. Helicity control of π -stacked assemblies of oligo (para-phenylene) derivatives using photoresponsive chiral moieties at terminal sites. *Adv. Funct. Mater.* **2014**, *24*, 6166–6171.
- (26) Xue, S. X.; Xing, P. Y.; Zhang, J. B.; Zeng, Y. F.; Zhao, Y. L. Diverse role of solvents in controlling supramolecular chirality. *Chem. – Eur. J.* **2019**, *25*, 7426–7437.
- (27) Nandakumar, A.; Ito, Y.; Ueda, M. Solvent effects on the self-assembly of an amphiphilic polypeptide incorporating α -helical hydrophobic blocks. *J. Am. Chem. Soc.* **2020**, *142*, 20994–21003.
- (28) Wu, B.; Wu, H. W.; Zhou, Y. Y.; Zheng, D. X.; Jia, X. Y.; Fang, L.; Zhu, L. L. Controlling ultra-large optical asymmetry in amorphous molecular aggregations. *Angew. Chem., Int. Ed.* **2021**, *60*, 3672–3678.
- (29) Balakrishnan, K.; Datar, A.; Naddo, T.; Huang, J. L.; Oitker, R.; Yen, M.; Zhao, J. C.; Zang, L. Effect of side-chain substituents on self-

- assembly of perylene diimide molecules: morphology control. *J. Am. Chem. Soc.* **2006**, *128*, 7390–7398.
- (30) Li, X. J.; Huang, H.; Angunawela, I.; Zhou, J. D.; Du, J. Q.; Liebman-Pelaez, A.; Zhu, C. H.; Zhang, Z. J.; Meng, L.; Xie, Z. Q.; et al. Effects of short-axis alkoxy substituents on molecular self-assembly and photovoltaic performance of indacenodithiophene-based acceptors. *Adv. Funct. Mater.* **2020**, *30*, No. 1906855.
- (31) Qin, M. G.; Zhang, Y. Q.; Xing, C.; Yang, L.; Zhao, C. L.; Dou, X. Q.; Feng, C. L. Effect of Stereochemistry on Chirality and Gelation Properties of Supramolecular Self-Assemblies. *Chem. – Eur. J.* **2021**, *27*, 3119–3129.
- (32) Mondal, S.; Adler-Abramovich, L.; Lampel, A.; Bram, Y.; Lipstman, S.; Gazit, E. Formation of functional super-helical assemblies by constrained single heptad repeat. *Nat. Commun.* **2015**, *6*, 8615.
- (33) Wang, M. H.; Zhao, Y. R.; Zhang, L. M.; Deng, J.; Qi, K.; Zhou, P.; Ma, X. Y.; Wang, D.; Li, Z.; Wang, J. Q.; et al. Unexpected role of achiral glycine in determining the suprastuctural handedness of peptide nanofibrils. *ACS Nano* **2021**, *15*, 10328–10341.
- (34) Ariga, K.; Mori, T.; Kitao, T.; Uemura, T. Nanoarchitectonics: Supramolecular chiral nanoarchitectonics. *Adv. Mater.* **2020**, *32*, No. 1905657.
- (35) Liu, G. F.; Li, X.; Sheng, J. H.; Li, P. Z.; Ong, W. K.; Phua, S. Z.; Agren, H.; Zhu, L. L.; Zhao, Y. L. Helicity inversion of supramolecular hydrogels induced by achiral substituents. *ACS Nano* **2017**, *11*, 11880–111889.
- (36) van Bommel, K. J. C.; van der Pol, C.; Muizebelt, I.; Friggeri, A.; Heeres, A.; Meetsma, A.; Feringa, B. L.; van Esch, J. Responsive cyclohexane-based low-molecular-weight hydrogelator with modular architecture. *Angew. Chem., Int. Ed.* **2004**, *43*, 1663–1667.
- (37) Alberti, M.; Amat, A.; Aguilar, A.; Fernando, P. Methanol-methanol and methanol-water systems: the intermolecular interaction controlling the transition from small clusters to the liquid phase. *Phys. Chem. Chem. Phys.* **2017**, *19*, 16765–16774.
- (38) Basak, S.; Nandi, N.; Baral, A.; Banerjee, A. Tailor-made design of J- or H- aggregated naphthalenediimide-based gels and remarkable fluorescence turn on/off behaviour depending on solvent. *Chem. Commun.* **2015**, *51*, 780–783.
- (39) Peng, T.; Dang-i, A. Y.; Liu, J. Y.; Feng, C. L. [2+2] Photocycloaddition reaction regulated the stability and morphology of hydrogels. *Adv. Fiber Mater.* **2019**, *1*, 241–247.
- (40) Dou, X. Q.; Wu, B. B.; Liu, J. Y.; Zhao, C. L.; Qin, M. G.; Wang, Z. M.; Schönher, H.; Feng, C. L. Effect of chirality on cell spreading and differentiation: from chiral molecules to chiral self-assembly. *ACS Appl. Mater. Interfaces* **2019**, *11*, 38568–38577.
- (41) Liu, B.; Han, L.; Che, S. A. Formation of enantiomeric impeller-like helical architectures by DNA self-assembly and silica mineralization. *Angew. Chem., Int. Ed.* **2012**, *51*, 923–927.
- (42) Hamley, I. W.; Castelletto, V. Small-angle scattering of block copolymers in the melt, solution and crystal states. *Prog. Polym. Sci.* **2004**, *29*, 909–948.
- (43) Riwar, L. J.; Trapp, N.; Kuhn, B.; Diederich, F. Substituent effects in parallel-displaced π - π stacking interactions: distance matters. *Angew. Chem., Int. Ed.* **2017**, *56*, 11252–11257.
- (44) Dou, X. Q.; Li, P.; Zhang, D.; Feng, C. L. C2-symmetric benzene-based hydrogels with unique layered structures for controllable organic dye adsorption. *Soft Matter* **2012**, *8*, 3231–3238.
- (45) Dou, X. Q.; Li, P.; Zhang, D.; Feng, C. L. RGD anchored C2-benzene based PEG-like hydrogels as scaffolds for two and three dimensional cell cultures. *J. Mater. Chem. B* **2013**, *1*, 3562–3568.
- (46) Syamala, P. P. N.; Soberats, B.; Görl, D.; Gekle, S.; Würthner, F. Thermodynamic insights into the entropically driven self-assembly of amphiphilic dyes in water. *Chem. Sci.* **2019**, *10*, 9358–9366.
- (47) Zhou, C. Q.; Ren, Y. Y.; Han, J.; Gong, X. X.; Wei, Z. X.; Xie, J.; Guo, R. Controllable supramolecular chiral twisted nanoribbons from achiral conjugated oligoaniline derivatives. *J. Am. Chem. Soc.* **2018**, *140*, 9417–9425.
- (48) Senthilkumar, T.; Asha, S. K. An easy ‘Filter-and-Separate’ method for enantioselective separation and chiral sensing of substrates using a biomimetic homochiral polymers. *Chem. Commun.* **2015**, *51*, 8931–8934.
- (49) Tang, H. T.; Yang, K. K.; Wang, K. Y.; Meng, Q.; Wu, F.; Fang, Y.; Wu, X.; Li, Y. G.; Zhang, W. C.; Luo, Y. F.; et al. Engineering a homochiral metal-organic framework based on an amino acid for enantioselective separation. *Chem. Commun.* **2020**, *56*, 9016–9019.